Available online at www.sciencedirect.com
SCIENCE DIRECT®
European Journal of Mechanics B/Fluids 24 (2005) 328–337

Vortex pair and Chaplygin cusps

Luca Zannetti [a], Sergei I. Chernyshenko [b,*]

[a] *Dipartimento di Ingegneria Aeronautica e Spaziale, Politecnico di Torino, Torino, Italy*
[b] *School of Engineering Sciences, University of Southampton, Southampton, SO17 1BJ, UK*

Received 23 September 2003; received in revised form 1 June 2004; accepted 16 September 2004

Available online 21 November 2004

Abstract

An example is given of a flow past two bodies with two trapped point vortices so that the pressure is constant over the entire body surface and the flow has no stagnation points. The flow is constructed from the flow past a pair of counter-rotating vortices by replacing the stagnation points with stagnation regions of constant pressure following the Chaplygin concept. The stagnation regions are then interpreted as bodies. The demonstration of the possibility of a flow without adverse pressure gradient on solid walls and without stagnation points adjacent to closed-streamline regions is important for the high-Reynolds-number asymptotic theory of flows with trapped vortices.

Keywords: Trapped vortex; Separated flow; Potential flow

1. Introduction

A problem of an ideal fluid flow past a body is normally formulated for a given body shape. The velocity and pressure distribution over the body surface is obtained from the solution. An inverse problem consists in determining the body shape for a given velocity or pressure distribution over the body surface. Inverse formulation is interesting because the velocity distribution determines the circulation and, via the Joukowski theorem, the lift, within the ideal fluid flow model. Velocity and pressure are related by the Bernoulli equation, so that prescribing the velocity is equivalent to prescribing the pressure and vice versa. It is important to prescribe such a velocity distribution so that the viscous boundary layer does not separate under the action of the corresponding pressure gradient. A boundary layer can separate only if the pressure increases along the surface in the direction of the flow. For this reason it is interesting to prescribe a favourable pressure gradient throughout, that is, such a pressure distribution that the pressure only decreases in the direction of the flow over the entire body surface. This pressure/velocity distribution can have non-zero circulation and, therefore, can produce lift. However, according to the Stepanov theorem [1–3], when the pressure gradient is favourable throughout or neutral (that is zero) the solution of the inverse problem inevitably gives the body contour with self-intersections.

It is possible to overcome the obstacle posed by the Stepanov theorem by extending the class of flows under consideration from purely potential flows to flows with trapped vortices. The simplest model of a flow with a trapped vortex is the potential flow past a body with a point vortex positioned in the flow field in such a way that its velocity is zero. The entire flow is therefore steady. Numerous examples of such flows have been considered [4–6]. An idea of such a flow can be seen in Fig. 4,

* Corresponding author.
E-mail addresses: luca.zannetti@polito.it (L. Zannetti), chernysh@soton.ac.uk (S.I. Chernyshenko).

0997-7546/$ – see front matter
doi:10.1016/j.euromechflu.2004.09.005

where there are two trapped vortices. It has been demonstrated [7] that if a flow with a single trapped vortex has only favourable or neutral pressure gradient over the entire body surface, the region of closed streamlines that contains the vortex has to be of an unrealistically complicated shape. Because of this, it seems quite likely that such flows simply do not exist. An example of a flow with two trapped vortices and with a favourable pressure gradient over the entire body surface was given in [3]. In this example the body had non-zero volume and generated lift, thus proving, in principle, that such flows are possible.

In the case of a non-separated flow past a streamlined body, the viscosity effects are concentrated in the thin boundary layer and in the wake. If it can be ensured that the boundary layer does not separate and that the wake does not break down, the general scheme of the inviscid flow is consistent with high-Reynolds-number asymptotics of the viscous flow. Breakdown of the wake can happen when the wake is under the action of an unfavourable pressure gradient. For example, this is the case when there are two streamlined bodies with a common symmetry line parallel to the main flow direction. If the downstream body does not have a sharp leading edge, a stagnation point should form in an inviscid flow on its upwind surface. The velocity on the symmetry line of the wake is always less than the velocity at the edge of the wake, where it is equal to the velocity of the inviscid flow. Since the latter tends to zero as the stagnation point of the inviscid flow is approached, the velocity on the symmetry line will become zero somewhere upstream from the stagnation point. This creates a singularity in the wake [14], which signifies reversal of the flow and the necessity to change the entire scheme of the inviscid flow. Wake breakdown is a well-known but rare phenomenon. In fact, the same physical mechanism often leads to the breakdown of the so-called recirculating boundary layers which are characteristic of flows with trapped vortices. A recirculating boundary layer consists of the boundary layer at the part of the body surface which is in immediate contact with the closed streamline region, and the mixing layer that develops along the separating streamline. Chernyshenko [15] (see also [7]) showed that velocity profile of a recirculating boundary layer always contains a region where the velocity is less than the velocity of the inviscid flow at the edge of the layer and, hence, a recirculating boundary layer inevitably develops singularities if the inviscid flow at the edge of the layer has a stagnation point. Such a flow cannot therefore be a consistent limit of the viscous flow as the Reynolds number tends to infinity: instead, the entire scheme of the inviscid flow has to be modified.

While the flow constructed in [3] has a favourable pressure gradient over the entire body surface, it also has a stagnation point at the rear of the region of the closed streamlines. Therefore, the recirculating boundary layer would develop a singularity in that flow. The present paper describes an example of such a configuration where the pressure gradient is neutral over all the solid boundaries and at the same time there are no stagnation points in the flow.

The idea of the present study is simple. Chaplygin [16] pointed out that any stagnation point in the potential flow can be replaced with a small stagnation zone, that is, with a region of constant pressure bounded by free streamlines. We apply this idea to a flow with two trapped vortices, and interpret the stagnation regions as bodies. Naturally, in this case the pressure over the entire body surface is constant. To produce an explicit example, we take a steady flow past a pair of counter-rotating vortices, and replace the two stagnation points that are present in this flow with stagnation regions, or bodies.

The flow is modelled by point vortices and potential flow. The study is carried out according to classical techniques based on complex potential definition, hodograph representation and conformal mapping.

2. Chaplygin cusp and hodograph representation

Briefly, the Chaplygin idea [16] is represented by the streamline patterns shown in Fig. 1. The potential flow impinging on a flat wall is considered. The stagnation point in Fig. 1(a) is replaced in Fig. 1(b) by a body of fluid at rest bounded by the free streamline arcs C-B and C-D.

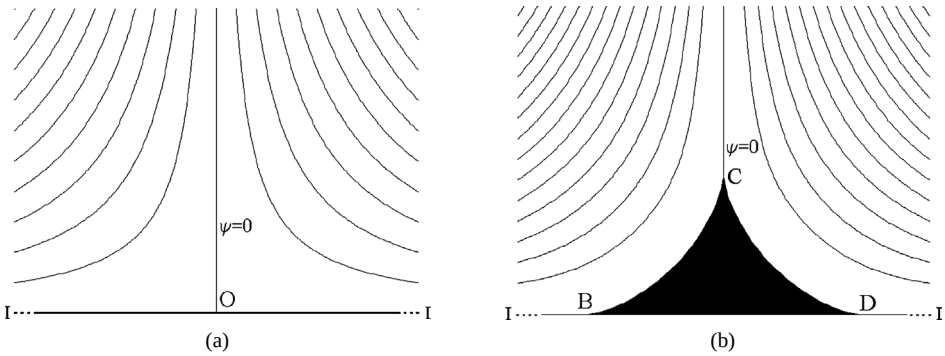

Fig. 1. (a) Stagnation flow. (b) Chaplygin cusp.

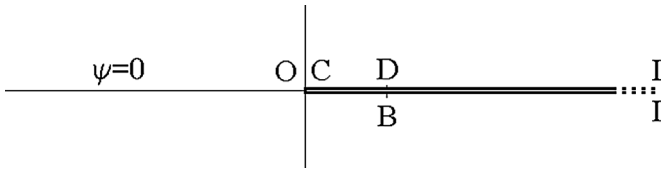

Fig. 2. $\psi = 0$ streamline on complex w and w_C planes.

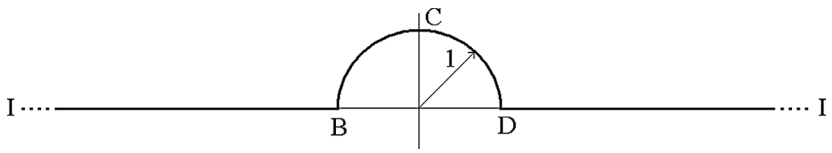

Fig. 3. Hodograph plane.

The shape of the free streamlines can be determined by means of the hodograph plane method (see for instance [17]).

Let $w = z^2$ be the complex potential of the flow impinging on an infinite wall, with the wall represented by the real axis and the flow taking place on the upper half-plane of the complex z-plane (with $z = x + \mathrm{i}y$), as shown in Fig. 1a. The stagnation streamline $\psi = 0$ coincides with the real axis of w-plane. As shown in Fig. 2, w-plane presents a branch cut on the positive real axis, with its upper and lower sides corresponding to the right and left portions of the wall, split by the stagnation point, respectively.

For a proper potential w_C, Fig. 2 is representative of $\psi = 0$ streamline of Fig. 1(b) as well. On the hodograph $\mathrm{d}w_C/\mathrm{d}z$-plane, the C-B and C-D free streamline arcs are constant velocity lines, that is circular arcs centered on the origin, while the solid portions I-B and D-I are straight lines, as shown in Fig. 3.

Fig. 2 can be mapped onto Fig. 3 by means of the analytic function

$$\frac{\mathrm{d}w_C}{\mathrm{d}z} = \mathrm{i}\sqrt{-w_C} + \sqrt{w_C - 1},$$

hence, integrating

$$\frac{\mathrm{d}z}{\mathrm{d}w_C} = \frac{1}{\mathrm{i}\sqrt{-w_C} + \sqrt{w_C - 1}}$$

provides the $z = z(w_C)$ relationship

$$z = \left(\frac{2}{3} - \frac{2w_C}{3}\right)\sqrt{-1 + w_C} + \frac{2\mathrm{i}}{3}\sqrt{-w_C}\, w_C + const$$

that allows C-B and C-D arc shapes to be determined.

Chaplygin was the first to point out that, since in the vicinity of the stagnation point any potential flow is similar to the flow considered in this section, if there exists a potential flow with a stagnation point then there exists a similar flow with a constant-pressure region bounded by free streamlines instead of the stagnation point.

3. Inverse problem solution for the vortex pair flow

The idea of the present study is simple. Chaplygin's concept is applied to the flow due to a vortex pair standing in equilibrium in an incoming uniform flow. Following Chaplygin's idea, the two stagnation points of this flow are replaced by two bodies of fluid at rest. These fluid bodies can hence be interpreted as solid bodies capable of trapping a vortex pair in a flow in which there are no stagnation points and the pressure on the body surfaces has a constant distribution. The flow field is sketched in Fig. 4, with the diamond shaped bodies representing the solid bodies trapping the vortices.

In the pure vortex pair flow with prescribed vortex locations, the vortex pair stands in equilibrium only for a certain ratio of the vortex circulation to the velocity at infinity. As it will be shown in what follows, there is a one-parameter family of body shapes capable of trapping a vortex pair, and for each body geometry the vortices remain stationary also only for a certain value of the ratio of the circulation to the velocity at infinity.

The study is carried out using the classical techniques based on complex potential definition, hodograph representation and conformal mapping.

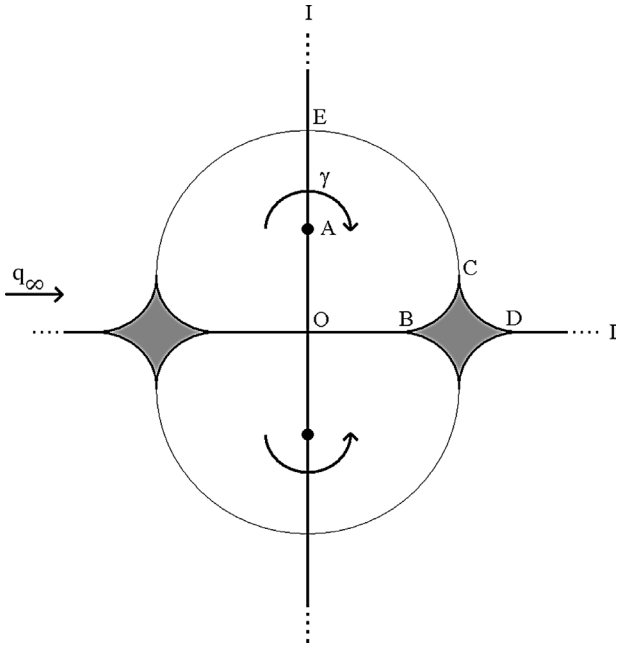

Fig. 4. Outline of the physical plane.

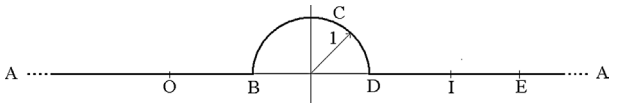

Fig. 5. Hodograph $\mathrm{d}w/\mathrm{d}z$-plane.

Let assume the physical plane sketched in Fig. 4 as the complex z-plane. The figure is symmetrical with respect to the real and imaginary axes. Point I is located at infinity. We want to design the arcs BC and CD for a vortex standing at point A, with circulation $\gamma < 0$ and asymptotic flow velocity q_∞, in a way that the flow velocity is constant ($|q| = q_0$) along them.

In order to express the problem in a non-dimensional form, let us assume $q_{\mathrm{ref}} = q_0$ as the reference velocity and the quantity $l_{\mathrm{ref}} = |\gamma|/(2\pi q_0)$ as the reference length. From now on, all the quantities will be considered as normalised with respect to these reference values. Specifically, the normalised flow velocity along the BC and CD arcs is $|q| = 1$ and the normalised vortex circulation is $\gamma = -2\pi$.

Fig. 5 shows the contour corresponding to the $AOBCDIEA$ line of the z-plane on the hodograph $\mathrm{d}w/\mathrm{d}z$-plane. Point A is the vortex location and, as a consequence, is located at infinity of the hodograph plane.

Fig. 6 shows the $AOBCDIEA$ line mapped onto the complex potential $w = \varphi + \mathrm{i}\psi$ plane. The points E, C, B, O, D, I belong to the same $\psi = \psi_O$ streamline, with $\varphi_O - \varphi_E = \gamma/2$. Line AEI is mapped onto the constant potential line $\varphi = \varphi_E$ that extends from $\psi_A = -\infty$ to $\psi_I = +\infty$ and line OA is mapped onto the constant potential line $\varphi = \varphi_O$ that extends from $\psi_A = -\infty$ to ψ_O.

Both the $AOBCDIEA$ contours of the $\mathrm{d}w/\mathrm{d}z$-plane and the w-plane can be mapped onto the real axis of an auxiliary λ-plane, as shown in Fig. 7.

The mapping from the $\mathrm{d}w/\mathrm{d}z$ plane to the λ-plane can be obtained by using the Joukowski transformation

$$\lambda = \frac{1}{2}\left(\frac{\mathrm{d}w}{\mathrm{d}z} + \frac{1}{\mathrm{d}w/\mathrm{d}z}\right)$$

whose inverse is

$$\frac{\mathrm{d}w}{\mathrm{d}z} = \lambda + \sqrt{\lambda^2 - 1}. \tag{1}$$

The mapping from the w-plane to the λ-plane can be accomplished by using the Schwartz–Christoffel transformation. The contour of w-plane can be in fact seen as a polygon with vertices A, O, C, I (A, I located at infinity) and with angles $\hat{\mathrm{A}} = \pi$,

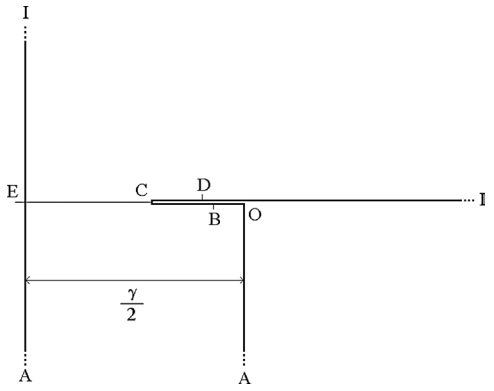

Fig. 6. w-plane.

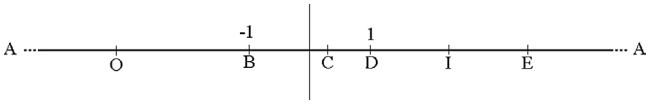

Fig. 7. λ-plane.

$\widehat{\mathrm{O}} = \pi/2$, $\widehat{\mathrm{C}} = -\pi$, $\hat{\mathrm{I}} = 3/2\pi$. The Schwartz–Christoffel transformation maps the polygon contour onto the real axis of λ-plane and its interior onto the upper half λ-plane. The mapping derivative is

$$\frac{\mathrm{d}w}{\mathrm{d}\lambda} = -\mathrm{i}\frac{\lambda - \lambda_C}{\sqrt{(\lambda - \lambda_O)(\lambda - \lambda_I)^3}}, \tag{2}$$

where $\lambda_O, \lambda_C, \lambda_I$ are the images of the vertices O, C, I on the real axis of λ-plane, their values define the polygon side lengths.

From (1) and (2), we obtain

$$\frac{\mathrm{d}z}{\mathrm{d}\lambda} = \frac{\mathrm{d}w}{\mathrm{d}\lambda}\Big/\frac{\mathrm{d}w}{\mathrm{d}z} = -\mathrm{i}\frac{\lambda - \lambda_C}{\sqrt{(\lambda - \lambda_O)(\lambda - \lambda_I)^3}(\lambda + \sqrt{\lambda^2 - 1})}, \tag{3}$$

whose integration

$$z(\lambda) = \int \frac{\mathrm{d}z}{\mathrm{d}\lambda}\,\mathrm{d}\lambda \tag{4}$$

provides a parametric representation of the cusp shape.

4. Determination of the $\lambda_O, \lambda_C, \lambda_I$ parameters

According to the previous analysis, there are three λ_O, λ_C and λ_I parameters to be found. In order to make Figs. (4), (5), and (6) consistent, they have to satisfy the constraints:

$$\lambda_O \leqslant -1, \qquad -1 \leqslant \lambda_C \leqslant 1, \qquad \lambda_I \geqslant 1. \tag{5}$$

In what follows it is shown that the vortex equilibrium condition prescribes the relationship $3\lambda_I - 2\lambda_C + \lambda_O = 0$ and, as a consequence, the problem has two degrees of freedom. It is also shown that the condition that lines $O - B$ and $D - I$ of Fig. 4 belong to the same axis, that is, $\mathrm{Im}(z_B) = \mathrm{Im}(z_D)$, implies a further relationship between the parameters and therefore the problem that satisfies this condition has one degree of freedom. A solution with $\mathrm{Im}(z_B)$ greater (less) than $\mathrm{Im}(z_D)$ is in fact consistent with Fig. 5, but the y-symmetry of the flow implies that the line $O - B$ ($D - I$) has to be considered as a solid wall with non-constant velocity on it. Therefore, as a consequence of the x-symmetry, an adverse pressure gradient will be present on this solid wall.

In order to discuss the vortex equilibrium condition, we determine the transformation $z = z(\zeta)$ that maps the upper flow region of the z-plane that is represented in Fig. 4 onto the upper half of the ζ-plane in such a way that $\zeta_O = 0$ and $\zeta_I = \infty$. The transformation can be expressed as a mapping chain $z \to \lambda \to \zeta$, or in equivalent form, as a parametric representation $z = z(\lambda)$, $\zeta = \zeta(\lambda)$, where the complex variable λ is the parameter.

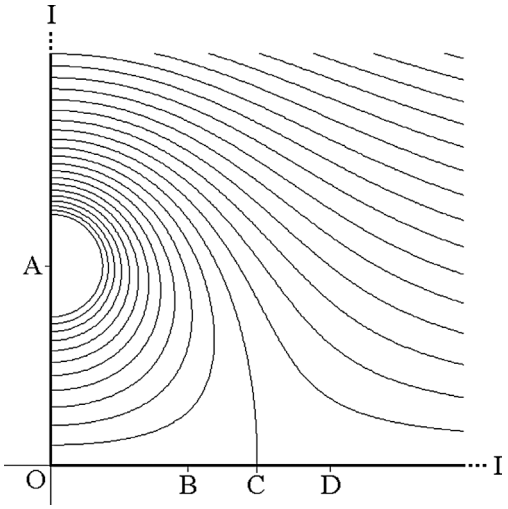

Fig. 8. ζ-plane.

The mapping $z = z(\lambda)$ has already been determined, it is given by (4). The transformation $\zeta = \zeta(\lambda)$ is given by the mapping

$$\zeta = \mathrm{i}\sqrt{\frac{\lambda - \lambda_O}{\lambda - \lambda_I}}, \tag{6}$$

which maps the upper half of the λ-plane onto the upper right quarter of the ζ-plane with the streamline $OBCDI$ and its symmetric upstream portion of the z-plane mapped onto the real axis of ζ-plane. Point O is mapped onto the origin at $\zeta = 0$, point I at infinity is mapped onto the point at infinity $\zeta = \infty$ and the vortex location A is mapped onto $\zeta = \mathrm{i}$, as shown in Fig. 8.

The complex potential w on the ζ-plane is the potential due to a vortex with circulation $\gamma = -2\pi$ located at $\zeta = \mathrm{i}$, to its reflected image with respect to the real axis and to an asymptotic uniform flow, that is:

$$w = Q_\infty \zeta + \mathrm{i}\log\left(\frac{\zeta - \mathrm{i}}{\zeta + \mathrm{i}}\right) \tag{7}$$

with

$$Q_\infty = q_\infty \lim_{\zeta\to\infty} \frac{\mathrm{d}z}{\mathrm{d}\zeta},$$

where, according to (1), $q_\infty = \lambda_I + \sqrt{\lambda_I^2 - 1}$.

The complex velocity on the transformed ζ-plane is therefore

$$\frac{\mathrm{d}w}{\mathrm{d}\zeta} = Q_\infty + \mathrm{i}\left(\frac{1}{\zeta - \mathrm{i}} - \frac{1}{\zeta + \mathrm{i}}\right). \tag{8}$$

The mapping derivative $\mathrm{d}z/\mathrm{d}\zeta = (\mathrm{d}z/\mathrm{d}\lambda)/(\mathrm{d}\zeta/\mathrm{d}\lambda)$ can be expressed parametrically as a function of λ, that is, according to (3) and the λ-derivative of (6):

$$\frac{\mathrm{d}z}{\mathrm{d}\zeta} = 2\frac{\lambda - \lambda_C}{(\lambda + \sqrt{\lambda^2 - 1})(\lambda_I - \lambda_O)}, \tag{9}$$

therefore

$$Q_\infty = q_\infty \lim_{\lambda\to\lambda_I} \frac{\mathrm{d}z}{\mathrm{d}\zeta} = 2\frac{\lambda_I - \lambda_C}{\lambda_I - \lambda_O}.$$

According to the Routh rule [18,19], the velocity of the vortex located at z_A is expressed by:

$$\dot{z}_A = \left[\zeta_A' - \frac{\gamma}{4\pi\,\mathrm{i}}\frac{\mathrm{d}}{\mathrm{d}\zeta}\left(\log\frac{\mathrm{d}z}{\mathrm{d}\zeta}\right)_{\zeta=\mathrm{i}}\right]\left(\frac{\mathrm{d}\zeta}{\mathrm{d}z}\right)_{\zeta=\mathrm{i}}, \tag{10}$$

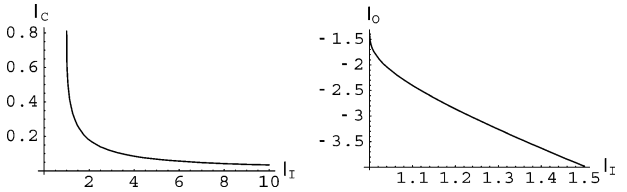

Fig. 9. $\lambda_C(\lambda_I)$, $\lambda_O(\lambda_I)$ for aligned $O-B$ and $D-\infty$ lines.

where ζ'_A is the velocity a free vortex with circulation -2π located at $\zeta(z_A)=\mathrm{i}$ would have on the ζ-plane, that is

$$\zeta'_A = Q_\infty - \frac{1}{2} = \frac{3\lambda_I - 4\lambda_C + \lambda_O}{2(\lambda_I - \lambda_O)}. \tag{11}$$

As

$$\frac{\mathrm{d}}{\mathrm{d}\zeta}\left(\log\frac{\mathrm{d}z}{\mathrm{d}\zeta}\right)_{\zeta=\mathrm{i}} = \lim_{\lambda\to\infty}\frac{\frac{\mathrm{d}}{\mathrm{d}\lambda}(\log(\mathrm{d}z/\mathrm{d}\zeta))}{\mathrm{d}\zeta/\mathrm{d}\lambda} = 2\mathrm{i}\frac{\lambda_C}{\lambda_I-\lambda_O}$$

the vortex equilibrium condition $\dot{z}_A = 0$ yields

$$3\lambda_I - 2\lambda_C + \lambda_O = 0. \tag{12}$$

The condition that the $O-B$ and the $D-\infty$ lines are aligned on the same axis is expressed by the condition $\mathrm{Im}(z_B)=\mathrm{Im}(z_D)$, that is, according to (3)

$$\mathrm{Im}\left(\int_{\lambda_B}^{\lambda_D}\frac{\mathrm{d}z}{\mathrm{d}\lambda}\mathrm{d}\lambda\right) = \int_{-1}^{1}\frac{(\lambda_C-\lambda)\sqrt{1-\lambda^2}}{\sqrt{(\lambda-\lambda_O)(\lambda_I-\lambda)^3}}\,\mathrm{d}\lambda = 0, \tag{13}$$

which can be expressed analytically by means of elliptic functions. This condition can be set in the form $\lambda_C=\lambda_C(\lambda_I)$ or $\lambda_O=\lambda_O(\lambda_I)$ by numerical evaluation once λ_O or λ_I is replaced by means of (12). Plots of $\lambda_C(\lambda_I)$ and $\lambda_O(\lambda_I)$ are shown in Fig. 9. Function $\lambda_C(\lambda_I)$ is monotone and positive, and $\lim_{\lambda_I\to\infty}\lambda_C = 0$. Moreover, since the integrand in (13) is positive for $\lambda<\lambda_C$, condition (13) cannot be satisfied for $\lambda_C = 1$. Therefore, the intervals in which (13) can be satisfied are

$$\lambda_O < -1, \qquad 0<\lambda_C<1, \qquad 1<\lambda_I. \tag{14}$$

5. Examples

The first example shown in Fig. 10 is relevant to a generic cusp that obeys the vortex equilibrium condition (12) and does not comply with the $\mathrm{Im}(z_B)=\mathrm{Im}(z_D)$ condition (13). The parameter choice is $\lambda_I = 1.5$, $\lambda_C = 0$ and, according to (12), $\lambda_O = -4.5$. The cusp geometry has been obtained by numerical integration of (3). The vortex location z_A has been determined by evaluating the integral

$$z_A = \int_0^{\mathrm{i}}\frac{\mathrm{d}z}{\mathrm{d}\zeta}\,\mathrm{d}\zeta,$$

where $\mathrm{d}z/\mathrm{d}\zeta$ is given by (9) and is expressed as a function of ζ by inverting (6).

Enforcing condition (13) for the same choice of $\lambda_I = 1.5$, the other two parameters are $\lambda_C = 0.258863$ and $\lambda_O = -3.98227$. The resulting cusp geometry and velocity distribution are shown in Figs. 11 and 12, respectively.

As stated in the previous section, there is a one-parameter family of cusps that satisfies both conditions (12) and (13) that can be represented by the choice of $\lambda_I > 1$. The larger the λ_I value is, the smaller the $|\mathrm{Im}(z_C)/z_A|$ ratio results. Fig. 13 shows the cusp geometry for $\lambda_I = 20$. It can be inferred that for $\lambda_I\to\infty$ the cusp tends to vanish and the flow field tends to the pure vortex pair flow with a stagnation point in λ_C.

On the other hand, for $\lambda_I\to 1$ the cusp geometry tends to a closed cavity as Fig. 14, pertinent to $\lambda_I = 1.001$, shows.

One could think of designing a trapping vortex cavity with constant pressure along its solid wall by choosing $\lambda_O = -1$ and as a consequence of (12) and (5) $\lambda_C = \lambda_I = 1$. This is a singular parameter set which should be considered as a limit. Once condition (13) is relaxed, one can take $\lambda_C = 1$ and the limit cusp configuration for $\lambda_O\to -1$ can be considered. By choosing

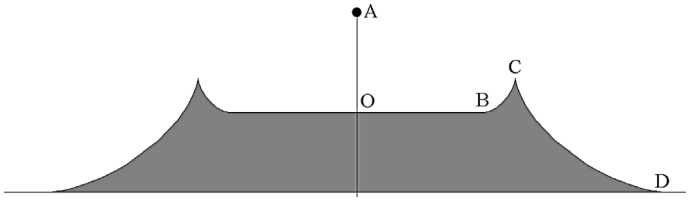

Fig. 10. Cusp shape and vortex location for $\lambda_I = 1.5$, $\lambda_C = 0$ and $\lambda_O = -4.5$.

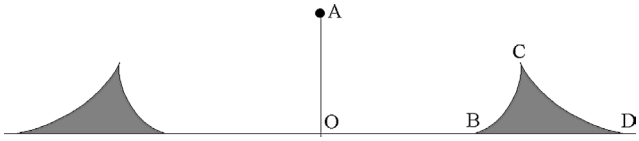

Fig. 11. Cusp shape and vortex location for $\lambda_I = 1.5$, $\lambda_C = 0.258863$ and $\lambda_O = -3.98227$.

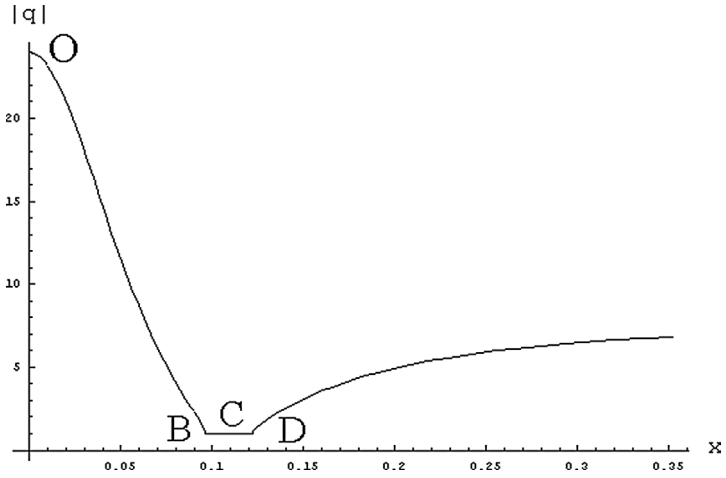

Fig. 12. Flow velocity distribution for $\lambda_I = 1.5$, $\lambda_C = 0.258863$ and $\lambda_O = -3.98227$.

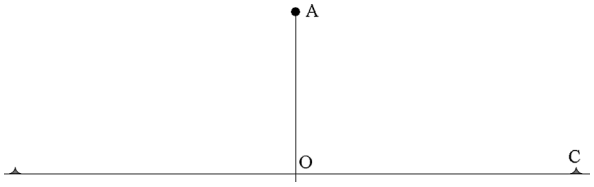

Fig. 13. Cusp shape and vortex location for $\lambda_I = 20$, $\lambda_C = 0.0164$ and $\lambda_O = -59.967$.

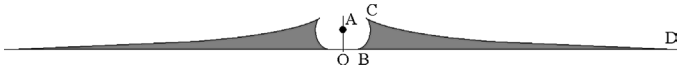

Fig. 14. Cusp shape and vortex location for $\lambda_I = 1.001$, $\lambda_C = 0.751$ and $\lambda_O = -1.5$.

λ_O close to -1, it is possible to infer that the cusp tends to the trivial configuration shown in Fig. 15, that is a vortex on the center of a closed circular cavity and a uniform flow tangent to the cavity.

The flow configuration for $\lambda_C = 1$, $\lambda_O = -1.015$ and, according to (12), $\lambda_I = 1.005$, shown in Fig. 16, supports this conjecture.

In order to give a complete picture of the flow field streamlines, direct numerical integration of the $\mathrm{d}w/\mathrm{d}z$ is not convenient. A complete picture of the flow field once the solid wall shape is computed, is preferably obtained by mapping the upper portion

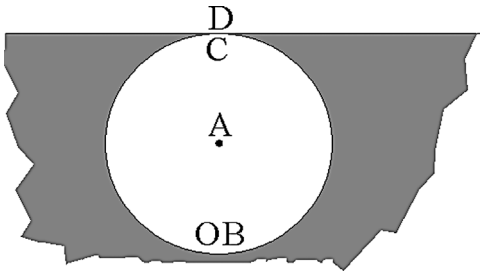

Fig. 15. Limit configuration for $\lambda_O = -1$, $\lambda_C = 1$ and $\lambda_I = 1$.

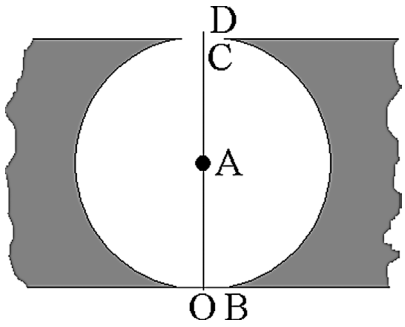

Fig. 16. Cusp shape and vortex location for $\lambda_C = 1$, $\lambda_O = -0.015$ and $\lambda_I = 1.005$.

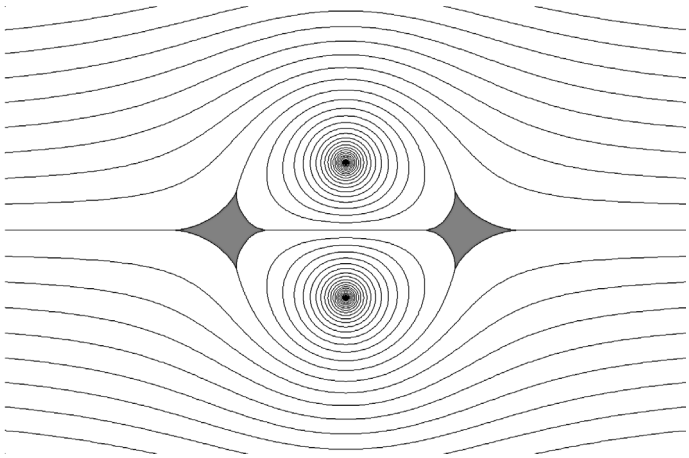

Fig. 17. Streamline pattern and body shape for $\lambda_I = 1.5$, $\lambda_C = 0.258863$ and $\lambda_O = -3.98227$.

of the z-plane bounded by the cusp outside the unit circle of the complex σ-plane. In short, the mapping chain $z \to \mu \to \nu \to \sigma$ is used with

$$\mu = \frac{z+c}{z-c}, \qquad \frac{\nu-1}{\nu+1} = \left(\frac{\mu-\mu_C}{\mu+\mu_C}\right)^2, \qquad \nu = b + \sigma \exp \sum_{j=0}^{\infty} a_j \sigma^{-j},$$

where a_j, b, and c are constants. The third equation is the Theodorsen–Garrick transformation, where the a_j coefficients are determined according to a trial and error process as described by Ives [13], while b and c are arbitrary and chosen in such a way that $\sigma_I = -1$, $\sigma_O = 1$, $\mathrm{Im}(\sigma_A) = 0$. The complex potential on the σ-plane is therefore

$$w = \frac{\mathrm{i}M}{\sigma+1} + \mathrm{i}\log\left(\frac{\sigma-\sigma_A}{\sigma-1/\sigma_A}\right)$$

with M determined by the Kutta condition $(\mathrm{d}w/\mathrm{d}\sigma)_{\sigma_C} = 0$. The correctness of the process can be checked by verifying that $(\mathrm{d}w/\mathrm{d}\sigma)/(\mathrm{d}z/\mathrm{d}\sigma)$ is equal to $\mathrm{d}w/\mathrm{d}z$ computed by (1) at the cusp points.

The streamline pattern pertinent to the cusp geometry of Fig. 11 is represented in Fig. 17 on the entire z-plane.

6. Concluding remarks

The constructed flow has a plane of symmetry parallel to the flow direction at infinity. For this reason the bodies do not generate lift. However, it seems obvious that, in principle, lift can be generated simply by prescribing non-constant pressure (but with favourable a gradient) and deviating from symmetry.

Strictly speaking, a boundary layer can remain attached even when the pressure increases in the direction of the flow. In order to determine whether separation has occurred one needs to calculate the boundary layer. The advantage of a configuration

with a favourable pressure gradient consists in the possibility of ensuring an attached flow without the analysis of the viscous boundary layers. Similarly, it is possible to construct flows with trapped vortices which are valid high-Reynolds-number limits of certain viscous flows even when there are regions of the adverse pressure gradient, and also similarly, it is convenient to be able to ensure the absence of separation/breakdown of thin viscous layers without analysing them in detail.

Naturally, the model of an ideal fluid flow with trapped point vortices is rather far from reality. The model of ideal fluid can be used only at high Reynolds numbers, but then the flows with eddies should be expected to be unstable. On the other hand, flow stability depends on the geometry, and stabilisation with active control is a possibility, however these aspects are well beyond the scope of the present study. More information on stability and control of flows with trapped vortices can be found in the literature [8–12].

Even within a limited scope of steady flows, trapped point vortices remain a very idealised model. A viscous flow with trapped vortices would tend to a Batchelor-model flow [7]. However, as far as a demonstration, in principle, of the possibility of a certain type of a flow is concerned, point vortices are a legitimate tool. The results that have been obtained demonstrate that there is no general theorem, like the Stepanov theorem or the theorem concerning flows with a single trapped vortex proved by Bunyakin et al. [7], which would not allow construction of flows with a favourable pressure gradient on the solid boundaries and without stagnation points on the eddy boundary. These two requirements are the only major limitations imposed on the inviscid flow by the high-Reynolds-number asymptotic theory of viscous flow with trapped vortices. Therefore, the obtained result demonstrates that it is possible to construct families of inviscid flows with trapped vortices which can contain the true high-Reynolds-number limit of the viscous flow without detailed analysis of viscous effects.

Acknowledgements

The research collaboration that resulted in the present paper was supported in part by a Royal Society grant 13872 under the European Science Exchange Programme.

References

[1] F.G. Avhadiev, D.V. Maklakov, A theory of pressure envelopes for hydrofoils, Ship Technology Research 42 (1995) 81–102.
[2] A.M. Elizarov, N.B. Il'inskiy, A.V. Potashev, Mathematical Methods of Airfoil Design, Akademie Verlag, Berlin, 1997.
[3] S.I. Chernyshenko, B. Galletti, A. Iollo, L. Zannetti, Trapped vortices and a favourable pressure gradient, J. Fluid Mech. 482 (2003) 235–255.
[4] M.K. Huang, C.Y. Chow, Trapping of a free vortex by Joukowski airfoils, AIAA J. 20 (3) (1982) 292–298.
[5] V.J. Rossow, Lift enhancement by an externally trapped vortex, J. Aircraft 15 (9) (1978) 618–625.
[6] P.G. Saffmann, J.S. Sheffield, Flow over a wing with an attached free vortex, Stud. Appl. Math. 57 (1977) 107–117.
[7] A.V. Bunyakin, S.I. Chernyshenko, G.Yu. Stepanov, High-Reynolds-number Batchelor-model asymptotics of a flow past an airfoil with a vortex trapped in a cavity, J. Fluid Mech. 358 (1998) 283–297.
[8] J.M. Wu, J.Z. Wu, Vortex lift at a very high angle of attack with massively separated unsteady flow, in: R. Kawamura, Y. Aihara (Eds.), Fluid Dynamic of High Angle of Attack. IUTAM Symp. Tokyo, Japan, September 13–17, 1992, Springer, 1992, p. 34.
[9] J.Z. Wu, X.Y. Lu, A.G. Denny, M. Fan, J.M. Wu, Post-stall flow control on an airfoil by local unsteady forcing, J. Fluid Mech. 371 (1998) 21–58.
[10] S.I. Chernyshenko, Stabilization of trapped vortices by alternating blowing-suction, Phys. Fluids 7 (4) (1995) 802–807.
[11] A. Iollo, L. Zannetti, Optimal control of a vortex trapped by an airfoil with a cavity, Flow, Turbulence and Combustion 65 (2000) 417–430.
[12] C. Min, H. Choi, Suboptimal feedback control of vortex shedding at low Reynolds numbers, J. Fluid Mech. 401 (1999) 123–156.
[13] D.C. Ives, A modern look at conformal mapping, including multiply connected regions, AIAA J. 14 (1976) 1006–1011.
[14] Vik.V. Sychev, On asymptotic theory of laminar separation from moving surface, Prikl. Mat. Mekh. 48 (2) (1984) 247–253 (In Russian). For English translation see J. Appl. Math. Mech.
[15] S.I. Chernyshenko, Separated flow over a backward-facing step whose height is much greater than the thickness of the lower sublayer of the interaction zone, Izv. Akad. Nauk SSSR Mekh. Zhidk. Gaza 4 (1991) 25–30 (In Russian). For English translation see Fluid Dynamics.
[16] M.I. Gurevich, The Theory of Jets in an Ideal Fluid, Pergamon Press, Oxford, 1966.
[17] H. Lamb, Hydrodinamics, vol. 12, Dover, New York, 1932, 94–104, Chapter IV.
[18] E.J. Routh, Some applications of conjugate functions, Proc. London Math. Soc. 12 (1881).
[19] P.G. Saffmann, Vortex Dynamics, Cambridge University Press, 1992, 123–124, Chapter 7.